International Journal of Mathematics Trends and Technology
ISSN: 2231-5373/ https://doi.org/10.14445/22315373/IJMTT-V72I8P103

Volume 72 Issue 8, 11-26, August 2026

Original Article

Analytical Approximation and an Efficient Adaptive Algorithm for a Delay-Induced Tumor–Immune–Normal Cell Model

S. Daniel[1], A.R. Manikandan[2]

[1]*P.G. & Research Department of Mathematics, Cardamom Planters' Association College, Bodinayakanur, Theni, Tamil Nadu, India.*

[1]*Corresponding Author : daniel.s@cpacollege.org*

Received: 21 June 2026 Revised: 24 July 2026 Accepted: 14 August 2026 Published: 29 August 2026

Abstract - *The delay-induced tumor–immune–normal cell model of Das et al. (Adv. Contin. Discrete Models 2022:15) established local and global stability results for the tumor-free equilibrium and a Hopf-bifurcation analysis for the coexisting equilibrium, supported by numerical simulation. The present note extends that work along two directions that were left open in the original paper. First, we derive a semi-analytical solution of the full nonlinear delay system using the classical method of steps combined with the Adomian Decomposition Method (ADM); we show that because the initial history is constant, the delay system reduces exactly to an ordinary differential system on the first characteristic interval [0,τ], which yields a genuine (verifiable) power-series solution rather than a purely numerical approximation, and we describe the recursive procedure that extends this construction to every subsequent interval [nτ,(n+1)τ]. Second, we identify and correct an order-reduction phenomenon that afflicts the naive fixed-step Runge–Kutta scheme used for this type of model (its empirical order drops from four to two because of low-order interpolation of the delayed argument), and we propose an adaptive continuous embedded Runge–Kutta 5(4) scheme with cubic-Hermite dense output ("ACDP-DDE") that restores fourth-order accuracy and reduces the number of function evaluations needed for a given accuracy by more than an order of magnitude. Both extensions are verified numerically against the equilibrium values, the critical delay $\tau_0 \approx 18.919$, and the qualitative dynamics (damped spiral, limit cycle, post-Hopf oscillation) reported in the original article.*

Keywords - *Adomian Decomposition Method (ADM), Adaptive Runge–Kutta Method, Delay Differential Equations (DDEs), HOPF Bifurcation, Tumor–Immune–Normal Cell Model.*

1. Introduction

Das et al. [1] studied a three-dimensional Delay Differential Equation (DDE) model of immune cells (M), tumor cells (H), and normal cells (R), obtained by inserting a discrete delay τ into the Michaelis–Menten recruitment term of the De Pillis–Radunskaya model [2]. They established: (i) positivity and boundedness of solutions; (ii) local and global asymptotic stability of the tumor-free equilibrium $P1$ under an explicit threshold condition; (iii) local stability of the coexisting equilibrium $P2$ for τ below a critical value $\tau 0$, loss of stability for $\tau > \tau 0$, and the occurrence of a Hopf bifurcation at $\tau = \tau 0$; and (iv) an estimate of the maximal delay length for which the resulting limit cycle remains stable. All of these results were illustrated purely by numerical simulation in Mathematical, and the paper explicitly notes that "the order of convergence of the methods employed, the CPU time required, etc., were not addressed."

This note supplies two complementary extensions that directly address that stated limitation: (a) an analytical (series) solution technique for the full nonlinear delay system, valid on successive characteristic intervals, together with a quantitative assessment of its radius of practical convergence; and (b) a new, provably more efficient numerical algorithm for simulating the model, together with an empirical convergence-order and efficiency study relative to a standard fixed-step scheme. Throughout, we use the parameter values of Table 1 in [1], reproduced here as Table 1, and the same initial data used in Figures 5–6 of [1]: M(0) = 0.7, H(0) = 0.01, R(0) = 0.993, with r1 = 0.4 (the regime in which the tumor-free equilibrium is unstable and the dynamics are governed by the coexisting equilibrium P2 and its Hopf bifurcation).

The mathematical model considered in the present study is based on the delay-induced tumor–immune model originally developed by Das et al. [1]. Therefore, the governing equations, biological interpretation of the model variables, parameter set, and the previously reported stability and bifurcation results are not claimed as new contributions of the present work. Das et al. [1] established positivity and boundedness of the model solutions, investigated the stability of the tumor-free and coexistence equilibria, identified a critical delay associated with Hopf bifurcation, and illustrated the resulting dynamical behavior through numerical simulations.

The novelty of the present work lies instead in the analytical and numerical treatment of the delay system. In particular, the following contributions distinguish the present study from the previous work.

1. Semi-analytical treatment of the nonlinear delay system. Exploiting the constant initial history, we show that the delayed tumor–immune system reduces exactly to a delay-free nonlinear ordinary differential system on the first characteristic interval [0, τ]. This permits the construction of an explicit semi-analytical solution using the Adomian Decomposition Method (ADM). The method is then extended successively to the later characteristic intervals through the method of steps.
2. Explicit analytical representation. Unlike the purely numerical treatment in the previous study, the present work provides explicit ADM components and a third-order truncated analytical representation of the solution on the first characteristic interval. Thus, the solution can be independently evaluated and used as a benchmark for numerical computations.
3. Identification of order reduction in the conventional numerical treatment. We demonstrate that a fixed-step fourth-order Runge–Kutta method combined with linear interpolation of the delayed state exhibits an empirical convergence order of approximately two. This reduction occurs because the second-order delay interpolation limits the overall accuracy of the nominally fourth-order Runge–Kutta scheme.
4. Order-matched adaptive numerical algorithm. To overcome this limitation, we implement an adaptive Dormand–Prince 5(4) scheme together with cubic-Hermite dense output for reconstruction of the delayed state. The resulting ACDP-DDE algorithm matches the accuracy of the delay interpolant with the underlying numerical integrator and restores approximately fourth-order convergence.
5. Quantitative computational-efficiency assessment. In addition to reproducing the qualitative dynamics, the present study compares the computational requirements of the conventional and proposed approaches. At comparable accuracy, the proposed method requires substantially fewer function evaluations than the fixed-step method, demonstrating a computational advantage that was not quantified in the previous study.
6. Independent verification of the delay-induced dynamics. The proposed algorithm is used to independently reproduce the pre-Hopf, critical-delay, and post-Hopf regimes. The equilibrium coordinates and critical delay are compared with the previously reported values, thereby providing an independent computational verification using a different numerical implementation.

Accordingly, the present work should not be interpreted as proposing a new biological tumor–immune model or as re-establishing the stability and Hopf-bifurcation results already available in the literature. Rather, its principal contribution is the development and verification of a semi-analytical solution framework and an order-matched numerical strategy for the existing delay-induced cancer model. This distinction is important because it separates the established biological and dynamical results from the new analytical, numerical, and computational contributions of the present study.

2. The Model and Notation

The governing system, reproduced from [1], is

$$\begin{aligned} \frac{dM}{dt} &= \mu + \frac{\rho M(t-\tau)H(t-\tau)}{\sigma + H(t-\tau)} - m_1 MH - d_1 M, \\ \frac{dH}{dt} &= r_1 H(1 - bH) - m_2 MH - h_1 HR, \\ \frac{dR}{dt} &= r_2 R(1 - R) - h_2 RH, \end{aligned} \tag{1}$$

with constant initial history $M(\xi) = M0$, $H(\xi) = H0$, $R(\xi) = R0$ for $\xi \in [-\tau, 0]$. The coexisting equilibrium $P2 = (M2, H2, R2)$ solves the algebraic system given in [1, Sec. 4]. Table 1 lists the parameter values used throughout (identical to [1, Table 1], Case 2: $r1 = 0.4$).

Table 1. Parameter values used in this note (identical to [1, Table 1], Case 2).

Parameter	μ	d_1	r_1	r_2	b	m_1	m_2	h_1	h_2	ρ	σ
Value	0.05	0.2	0.4	0.35	1.5	0.2	0.3	0.2	0.25	1	0.4

As an independent check before proceeding, we re-solved the equilibrium algebraic system numerically (Newton iteration

on the three fixed-point conditions) and obtained M2 = 0.579465, H2 = 0.0572258, R2 = 0.959124, agreeing with [1] to the six digits reported there. This equilibrium and the reported critical delay τ0 = 18.91866 are used as reference values in Sections 4–5.

2.1. Delay-Induced Stability and Hopf Bifurcation

The presence of the discrete time delay τ introduces an additional dynamical mechanism into the tumor–immune interaction system. In particular, an increase in the immune-response delay may destabilize the coexistence equilibrium and generate sustained oscillations. Therefore, in addition to the analytical approximation of the solution, it is important to examine the stability transition induced by the delay parameter.

Let

$$P_2 = (M_2, H_2, R_2) \tag{2}$$

denote the positive coexistence equilibrium. The equilibrium is independent of the delay parameter because, at equilibrium,

$$M(t-\tau) = M(t) = M_2, \; H(t-\tau) = H(t) = H_2 \tag{3}$$

Consequently, P2 is obtained from the algebraic system

$$\begin{aligned} 0 &= \mu + \frac{\rho M_2 H_2}{\sigma + H_2} - m_2 M_2 H_2 - d_1 M_2, \\ 0 &= r_1 H_2 (1 - b H_2) - m_2 M_2 H_2 - h_1 H_2 R_2, \\ 0 &= r_2 R_2 (1 - R_2) - h_2 R_2 H_2. \end{aligned} \tag{4}$$

For the parameter values considered in this study, the coexistence equilibrium is

$$P_2 = (0.579465, 0.0572258, 0.959124). \tag{5}$$

To investigate the effect of the delay, consider a small perturbation about the equilibrium,

$$M(t) = M_2 + x_1(t), \; H(t) = H_2 + x_2(t), \; R(t) = R_2 + x_3(t). \tag{6}$$

Substitution into the governing system and linearization about P2 gives the linear delay system

$$x'(t) = A_0 x(t) + A_1 x(t-\tau), \tag{7}$$

where

$$x(t) = \begin{pmatrix} x_1(t) \\ x_2(t) \\ x_3(t) \end{pmatrix} \tag{8}$$

The instantaneous Jacobian matrix is

$$A_0 = \begin{pmatrix} -d_1 - m_1 H_2 & -m_1 M_2 & 0 \\ -m_2 H_2 & r_1(1 - 2bH_2) - m_2 M_2 - h_1 R_2 & -h_1 H_2 \\ 0 & -h_2 R_2 & r_2(1 - 2R_2) \end{pmatrix} \tag{9}$$

while the delayed contribution is represented by

$$A_1 = \begin{pmatrix} \frac{\rho H_2}{\sigma + H_2} & \frac{\rho M_2 \sigma}{(\sigma + H_2)^2} & 0 \\ 0 & 0 & 0 \\ 0 & 0 & 0 \end{pmatrix} \tag{10}$$

Seeking solutions of the form

$$x(t) = v e^{\lambda t}, \; v \neq 0, \tag{11}$$

leads to

$$\left[\lambda I - A_0 - A_1 e^{-\lambda\tau}\right] v = 0. \tag{12}$$

Hence, the characteristic equation of the linearized delay system is

$$det\left[\lambda I - A_0 - A_1 e^{-\lambda\tau}\right] = 0. \tag{13}$$

Unlike an ordinary differential equation, the characteristic equation (13) contains the transcendental term $e^{-\lambda\tau}$ and therefore possesses infinitely many characteristic roots. The stability of the coexistence equilibrium is determined by the locations of these roots in the complex plane.

For sufficiently small delay, all characteristic roots have negative real parts and the coexistence equilibrium is locally asymptotically stable. As the delay increases, a conjugate pair of characteristic roots may cross the imaginary axis. Let

$$\lambda = i\omega, \ \omega > 0 \tag{14}$$

be a purely imaginary characteristic root. Substitution into Equation (13) gives

$$det[i\omega I - A_0 - A_1 e^{-i\omega\tau}] = 0. \tag{15}$$

Separating the real and imaginary parts of Equation (15) gives the corresponding frequency and critical-delay conditions. The smallest positive value of τ satisfying these conditions defines the first critical delay,

$$\tau_0 \approx 18.91866. \tag{16}$$

Thus, the delay-dependent stability behavior can be summarized as

$$\begin{cases} 0 \le \tau < \tau_0, & P_2 \text{ is locally asymptotically stable,} \\ \tau = \tau_0, & \text{a pair of characteristic roots lies on the imaginary axis,} \\ \tau > \tau_0, & P_2 \text{ loses stability, oscillatory dynamics emerge.} \end{cases} \tag{17}$$

At the critical value $\tau = \tau_0$, the crossing of a conjugate pair of complex eigenvalues through the imaginary axis provides the mechanism for a Hopf bifurcation. Consequently, the delay acts as a control parameter capable of transforming the long-time behavior of the tumor–immune system from convergence to the coexistence equilibrium to sustained oscillations.

For $\tau = 8 < \tau_0$, the numerical solution exhibits damped oscillations and approaches the coexistence equilibrium. At the critical value $\tau = \tau_0$, the oscillations persist and approach a periodic regime. For $\tau = 35 > \tau_0$, the equilibrium is unstable, and the system exhibits larger-amplitude oscillations. These three regimes provide an independent numerical illustration of the delay-induced stability transition predicted by the characteristic equation.

The numerical observations are therefore consistent with the delay-induced Hopf-bifurcation scenario:

$$stable\ equilibrium \rightarrow critical\ oscillatory\ state \rightarrow stable\ periodic\ oscillation, \tag{18}$$

as τ is increased through the critical value τ_0.

It should be emphasized that the present study uses the critical delay reported for the model parameter set under consideration and verifies the corresponding dynamical regimes numerically. A complete analytical Hopf-bifurcation theorem would additionally require a formal verification of the transversality condition.

$$\frac{d}{d\tau}\left(Re\ \lambda(\tau)\right)_{\tau=\tau_0} \neq 0, \tag{19}$$

together with the corresponding non-degeneracy conditions. These conditions distinguish a genuine Hopf bifurcation from a tangential stability crossing.

3. A Semi-Analytical Solution via the Method of Steps and Adomian Decomposition

3.1. The key structural simplification: constant history collapses the delay on the first interval

A nonlinear DDE with a discrete delay does not, in general, admit a closed-form solution. However, the method of steps (Bellman and Cooke) turns any DDE with a given history into a sequence of ordinary differential equations, one per interval of length τ, provided each ODE can itself be solved (exactly or approximately) before the next interval is entered. For system (1) with the constant history used in [1] and here, this reduction is exact and immediate: for $t \in [0, \tau]$, the delayed arguments

satisfy $t - \tau \leq 0$, so

$$M(t - \tau) \equiv M_0,\ H(t - \tau) \equiv H_0 \quad for\ all\ t \in [0, \tau]. \tag{20}$$

Substituting this into the first equation of (1), the delay term becomes the constant $K = \mu + \rho M_0 H_0/(\sigma + H_0)$, and system (1) reduces — exactly, not approximately — to the autonomous ODE system

$$\begin{aligned} M' &= K - d_1 M - m_1 MH, \\ H' &= r_1 H - r_1 b H^2 - m_2 MH - h_1 HR, \\ R' &= r_2 R - r_2 R^2 - h_2 RH, \end{aligned} \tag{21}$$

on $t \in [0, \tau]$, with initial data (M0, H0, R0). This is a genuine, delay-free polynomial ODE system, and it can be attacked with any classical semi-analytical technique. We use the Adomian Decomposition Method (ADM) because it handles the quadratic nonlinearities of (21) through simple recursive quadrature, without requiring a small parameter.

3.2. Adomian Decomposition of the Reduced System

Write $M = \Sigma_n M_n$, $H = \Sigma_n H_n$, $R = \Sigma_n R_n$ ($n = 0, 1, 2, \ldots$), with $M0 \equiv M(0)$, $H0 \equiv H(0)$, $R0 \equiv R(0)$ the actual initial values (reusing the symbol M0 etc. now for the zeroth ADM component, consistent with the initial condition). Applying the inverse operator $L^{-1}[\cdot] = \int_0^t (\cdot)\, ds$ to (21) and expanding the quadratic nonlinearities MH, H2, HR, R2 into the corresponding (bilinear, hence trivial) Adomian polynomials [25]

$$\begin{aligned} A_n &= \Sigma_{i=0}^{n} M_i H_{n-i}, B_n = \Sigma_{i=0}^{n} H_i H_{n-i}, \\ C_n &= \Sigma_{i=0}^{n} H_i R_{n-i}, E_n = \Sigma_{i=0}^{n} R_i R_{n-i}. \end{aligned} \tag{22}$$

The recursion is

$$\begin{aligned} M_{n+1} &= L^{-1}(K \cdot \delta_{n0} - d_1 M_n - m_1 A_n) \\ H_{n+1} &= L^{-1}(r_1 H_n - r_1 b B_n - m_2 A_n - h_1 C_n) \\ R_{n+1} &= L^{-1}(r_2 R_n - r_2 E_n - h_2 (H_n R\ terms)) \end{aligned} \tag{23}$$

for $n = 0, 1, 2, \ldots$, where δ_{n0} is the Kronecker delta. Each Mn, Hn, Rn is an explicit polynomial in t; truncating at n = N gives an N-th order approximate solution valid, as with any ADM/power-series method, on a neighbourhood of t = 0 whose practical radius must be checked numerically (Section 3.4).

3.3. Explicit Third-Order Solution for the Parameter set of Table 1

Using the parameter values of Table 1 and the initial data (M0, H0, R0) = (0.7, 0.01, 0.993) of [1, Figure 5–6], we evaluated the recursion (23) symbolically (computer algebra) up to N = 3. The resulting third-order truncated solution on the first characteristic interval is

$$\begin{aligned} M(t) &\approx 0.7 - 0.0743415\, t + 0.00751723\, t^2 - 0.000512159\, t^3, \\ H(t) &\approx 0.01 - 0.000146\, t + 0.000113044\, t^2 - 0.00000940288\, t^3, \\ R(t) &\approx 0.993 - 0.00004965\, t + 0.0000267514\, t^2 - 0.0000124548\, t^3, \end{aligned} \tag{24}$$

(coefficients rounded to 6 significant figures; exact rational coefficients were produced by the symbolic computation and are available on request). Because the reduction of Sec. 3.1 is exact, (24) is a bona fide truncated analytical solution of the full nonlinear delay system (1) on $[0, \tau]$ — it is not an approximation of the delay effect itself, only of the resulting (delay-free) polynomial ODE (21).

3.4. Extension to Later Intervals and Range of Validity

On the second interval $t \in [\tau, 2\tau]$, the delayed arguments $M(t - \tau)$, $H(t - \tau)$ now range over the Step-1 solution of Sec. 3.3, i.e. they are the explicit polynomial (24) evaluated at $t - \tau$. Substituting this explicit function of t into the first equation of (1) again yields a delay-free, non-autonomous (but explicitly known) ODE system, to which the same ADM recursion (23) applies verbatim, with K replaced by the now t-dependent forcing $\rho M(t-\tau)H(t-\tau)/(\sigma + H(t-\tau))$. Iterating, one obtains a well-defined analytical solution, order by order, on every interval $[n\tau, (n + 1)\tau]$, $n = 0, 1, 2, \ldots$ — this is precisely the method of steps, with ADM supplying the solver at each step instead of purely numerical quadrature.

We verified (24) against a high-accuracy numerical solution of the full delay system (Section 4) obtained with atol = rtol

= 10^{-11}. Table 2 reports the discrepancy at several times within and beyond the interval [0, τ] for τ = 8.

Table 2. Comparison of the third-order ADM approximation with the high-accuracy numerical solution of the full delay system for τ = 8. The table reports the values of M, H, and R at selected times and demonstrates the local accuracy of the truncated ADM representation

t	M (numeric)	M (ADM, ord.3)	H (numeric)	H (ADM, ord.3)	R (numeric)	R (ADM, ord.3)
0.5	0.664692	0.664652	0.009955	0.009954	0.992980	0.992980
1.0	0.632743	0.632678	0.009959	0.009958	0.992966	0.992965
1.5	0.603862	0.603695	0.010009	0.010004	0.992951	0.992944
2.0	0.577749	0.577318	0.010101	0.010085	0.992930	0.992908
3.0	0.532754	0.530846	0.010397	0.010326	0.992857	0.992756
4.0	0.496012	0.490190	0.010832	0.010623	0.992728	0.992432

As is typical for ADM and related series methods, the truncation error grows with t (the relative error in M grows from about 6×10^{-5} at t = 0.5 to about 1.2×10^{-2} at t = 4, within an interval of length τ = 8). Two standard remedies apply directly here and are noted for completeness rather than implemented in full: (i) Padé post-processing of the truncated series, which typically extends the useful interval several-fold without additional derivative information; and (ii) restarting the ADM recursion on sub-intervals of [0, τ] (a multistage ADM), which is algebraically identical to reducing the effective step of the method-of-steps grid. In the regime $\tau \geq \tau 0$ relevant to the Hopf bifurcation of [1], the sub-interval length required for engineering accuracy is small enough that a purely numerical treatment is preferable in practice, which motivates Section 4.

3.5. Existence, Positivity, Boundedness, and Error Estimates

To complement the semi-analytical construction, we establish the well-posedness and boundedness properties of the model and provide an error estimate for the truncated ADM representation. Consider the system

$$\begin{aligned} M' &= \mu + \frac{\rho M(t-\tau)H(t-\tau)}{\sigma + H(t-\tau)} - m_1 MH - d_1 M, \\ H' &= r_1 H(1 - bH) - m_2 MH - h_1 HR, \\ R' &= r_2 R(1 - R) - h_2 RH, \end{aligned} \tag{25}$$

with the non-negative initial history

$$M(\xi) = M_0,\ H(\xi) = H_0,\ R(\xi) = R_0,\ \xi \in [-\tau, 0]. \tag{26}$$

3.5.1 Existence and Uniqueness

For non-negative initial data, system (25) admits a unique solution on a maximal interval [0, Tmax).

Proof. For H ≥ 0, the delayed recruitment function

$$g(M_d, H_d) = \mu + \frac{\rho M_e H_e}{\sigma + H_e} \tag{27}$$

is continuously differentiable whenever σ + Hd > 0. Since σ > 0, the denominator is strictly positive for all non-negative values of Hd. The remaining terms in (25) are polynomial functions of the current variables M, H, and R. Therefore, the right-hand side is locally Lipschitz with respect to the state variables on every bounded subset of the non-negative phase space.

For 0 ≤ t ≤ τ, the delayed variables are determined by the initial history:

$$M(t - \tau) = M_0,\ H(t - \tau) = H_0. \tag{28}$$

Consequently, the delay system reduces exactly to the ordinary differential system given in Eq. (3). By the standard existence and uniqueness theorem for ordinary differential equations, a unique solution exists on the first characteristic interval [0, τ].

Once this solution has been constructed on [0, τ], its values provide the required history on [τ, 2τ]. Repeating this argument

successively on the characteristic intervals [nτ, (n + 1)τ] establishes a unique solution on the maximal interval [0, Tmax) on which the solution remains bounded.

3.5.2. Positivity of the Solution

If

$$M_0 \geq 0,\ H_0 \geq 0,\ R_0 \geq 0, \tag{29}$$

then

$$M(t) \geq 0,\ H(t) \geq 0,\ R(t) \geq 0, \tag{30}$$

for all t ∈ [0, Tmax).

Proof. Consider the boundary M = 0. From the first equation of (25), we obtain

$$M' = \mu + \frac{\rho M(t-\tau)H(t-\tau)}{\sigma + H(t-\tau)} \geq 0. \tag{31}$$

Therefore, the vector field does not point from the non-negative region into the region M < 0. Similarly, at H = 0,

$$H' = 0, \tag{32}$$

because every term in the second equation contains the factor H. Hence, H(t) cannot cross from H ≥ 0 into the negative region.

At R = 0,

$$R' = 0, \tag{33}$$

Since every term in the third equation contains the factor R R(t) also remains non-negative. Consequently, the non-negative orthant

$$\mathbb{R}^3_+ = \{(M,H,R) : M \geq 0, H \geq 0, R \geq 0\} \tag{34}$$

is positively invariant.

3.5.3. Boundedness of the Solution

For non-negative initial data, the solution of (25) remains bounded on every finite time interval. In particular,

$$0 \leq H(t) \leq max\left\{H_0, \frac{1}{b}\right\}, \tag{35}$$

and

$$0 \leq R(t) \leq max\{R_0, 1\}. \tag{36}$$

Proof. Since M, H, and R ≥ 0, the equation for H satisfies

$$H' = r_1 H(1 - bH) - m_2 MH - h_1 HR \leq r_1 H(1 - bH). \tag{37}$$

Comparison with the logistic equation

$$z' = r_1 z(1 - bz) \tag{38}$$

therefore gives

$$H(t) \leq max\left\{H_0, \frac{1}{b}\right\}. \tag{39}$$

Similarly, since H ≥ 0,

$$R' = r_2R(1 - R) - h_2RH \leq r_2R(1 - R). \tag{40}$$

Comparison with the corresponding logistic equation yields

$$R(t) \leq max\{R_0, 1\}. \tag{41}$$

For the immune-cell population M, observe that

$$\frac{H(t-\tau)}{\sigma + H(t-\tau)} \leq 1, \ H(t - \tau) \geq 0. \tag{42}$$

Hence,

$$M' \leq \mu + \rho M(t - \tau) - d_1M. \tag{43}$$

Let

$$M_k = \sup_{-\tau \leq s \leq k\tau} M(s). \tag{44}$$

On the characteristic interval [kτ, (k + 1)τ], inequality (43) gives

$$M(t) \leq M_k e^{-d_1(t-k\tau)} + \frac{\mu + \rho M_k}{d_1}\left(1 - e^{-d_1(t-k\tau)}\right). \tag{45}$$

Therefore, M(t) remains finite on every successive characteristic interval. Consequently, M, H, and R remain bounded on every finite time interval.

Since the right-hand side of the system is locally Lipschitz and the solution remains bounded, the solution can be continued indefinitely. Thus,

$$T_{\max} = \infty, \tag{46}$$

Moreover, the system possesses a unique global non-negative bounded solution.

3.5.4. ADM Truncation Error Estimate

Let

$$Y(t) = \begin{pmatrix} M(t) \\ H(t) \\ R(t) \end{pmatrix} \tag{47}$$

denote the exact solution on a characteristic interval. The ADM solution is represented in the form

$$Y(t) = \Sigma_{n=0}^{\infty} Y_n(t), \tag{48}$$

and its N-th order truncated approximation is defined by

$$Y^{(N)}(t) = \Sigma_{n=0}^{N} Y_n(t). \tag{49}$$

The corresponding truncation error is

$$E_N(t) = Y(t) - Y^{(N)}(t) = \Sigma_{n=N+1}^{\infty} Y_n(t). \tag{50}$$

Assume that, on $0 \leq t \leq T$, the ADM components satisfy

$$\|Y_n(t)\| \leq Cq^{n+1}t^{n+1}, \ C > 0, qT < 1. \tag{51}$$

Then, using (50),

$$\|E_N(t)\| \leq \Sigma_{n=N+1}^{\infty} \|Y_n(t)\| \leq C\, \Sigma_{n=N+1}^{\infty} (qt)^{n+1}. \quad (52)$$

Since qt < 1, the above geometric series converges and therefore

$$\|E_N(t)\| \leq \frac{(qt)^{N+2}}{1-qt},\ 0 \leq t \leq T, qt < 1. \quad (53)$$

Thus, the ADM truncation error decreases as the number of retained terms increases, provided that the solution remains inside the convergence interval of the decomposition series.

For the third-order approximation employed in Equation (6), namely

$$Y^{(3)}(t) = Y_0(t) + Y_1(t) + Y_2(t) + Y_3(t), \quad (54)$$

The corresponding remainder satisfies

$$\|Y(t) - Y^{(3)}(t)\| \leq \frac{(qt)^5}{1-qt}. \quad (55)$$

Equation (55) provides a local quantitative estimate for the error associated with the third-order ADM approximation. The estimate also explains the gradual increase in the discrepancy between the ADM approximation and the high-accuracy numerical solution as t moves away from the initial point.

3.6. Implications of the Delay-Induced Bifurcation

The delay parameter τ has a direct qualitative influence on the stability of the coexistence equilibrium. The characteristic equation (13) demonstrates that the delay enters the linearized dynamics through the transcendental factor $e^{-\lambda\tau}$. Consequently, increasing τ changes the location of the characteristic roots and may cause a conjugate pair of roots to cross the imaginary axis. For the parameter set considered here, this transition occurs at the critical value $\tau_0 \approx 18.91866$. The numerical simulations confirm the corresponding transition from damped oscillations for $\tau < \tau_0$ to sustained oscillatory behavior at and beyond the critical delay. Thus, the delay is not merely a temporal parameter in the model; it acts as a bifurcation parameter controlling the qualitative behavior of the tumor–immune interaction.

This delay-induced transition is biologically relevant because an increasing immune-response delay can cause the feedback between immune cells and tumor cells to become increasingly out of phase. When the delay is sufficiently small, the feedback remains sufficiently synchronized to stabilize the coexistence state. As the delay increases, the feedback becomes destabilizing and sustained oscillations may emerge. The numerical results for $\tau = 8$, $\tau = \tau_0$, and $\tau = 35$ illustrate these three dynamical regimes.

3.6.1. Remark on the Range of Validity

The error estimate (53) is a local estimate and requires the bound in (51). Therefore, it should not be interpreted as a global error estimate for arbitrarily large values of t. For longer time intervals, the ADM construction can be restarted on successive subintervals of the characteristic interval. This multistage implementation limits the growth of the truncation error and provides a controlled approximation over an extended time domain.

The above results establish the existence, uniqueness, positivity, and boundedness of the solution and provide a quantitative local error estimate for the ADM approximation. These analytical results complement the numerical convergence and efficiency analysis of the proposed ACDP-DDE scheme presented in the following section.

4. A New Adaptive Algorithm for the Delay System

4.1. Order Reduction in the Naive Scheme

The simulations in [1] were produced with Mathematica's built-in DDE solver, and no convergence or efficiency study was reported. A natural first candidate for an independent, transparent implementation is the classical method of steps with fourth-order Runge–Kutta (RK4) time-stepping and linear interpolation of the delayed argument between grid points (this is essentially the textbook "naive" DDE scheme). We implemented this scheme ("Method A") and measured its empirical order of convergence against a high-accuracy reference solution (atol = rtol = 10^{-13}). The result, summarised in Table 3, shows an empirical order of 2.0, not the 4.0 one would expect from RK4 alone.

Table 3. Empirical convergence of Method A (fixed-step RK4 + linear delay interpolation). Successive error ratios give an empirical order of 2.00–2.01, i.e. the scheme behaves as a second-order method overall

h	0.08	0.04	0.02	0.01	0.005
Error at T = 40 (τ = 8)	3.47×10^{-7}	8.66×10^{-8}	2.17×10^{-8}	5.41×10^{-9}	1.35×10^{-9}

This order reduction is a known phenomenon in the numerical analysis of DDEs [3]: the overall accuracy of a method-of-steps scheme is bounded above by the accuracy of the interpolant used to reconstruct the delayed argument between mesh points, regardless of the order of the underlying ODE stepper. Linear interpolation is only second-order accurate, and it therefore caps the whole scheme at second order, wasting the fourth-order accuracy that RK4 could otherwise deliver and forcing the use of unnecessarily small step sizes (equivalently, large numbers of function evaluations) to reach a target accuracy.

4.2. Proposed algorithm: ACDP-DDE

We propose an adaptive continuous Dormand–Prince DDE scheme (ACDP-DDE) that removes this bottleneck by matching the order of the delay-interpolant to the order of the ODE stepper, and by using an embedded pair for automatic step-size control:

4.2.1. Time-Stepping

The embedded Dormand–Prince 5(4) pair [4] advances the ODE, giving both a 5th-order solution and an independent 4th-order estimate for local error control.

4.2.2. Dense Output for the Delay Term

On every accepted step [tk, tk+1], we store (tk, tk+1, yk, yk+1, fk, fk+1) and reconstruct y(t) for $t_k \le t \le t_{k+1}$ using the cubic Hermite interpolant

$$y(t_k + sh) = h_{00}(s)\, y_k + he_0(s)\, hf_k + h_{01}(s)\, y_{k+1} + he_1(s)\, hf_{k+1},\ s = \frac{t - t_k}{h}, \tag{56}$$

with h00, he0, h01, he1 the standard Hermite basis functions. This interpolant matches both the value and the derivative at each node, giving fourth-order local accuracy — exactly matched to the discarded (4th-order) term of the embedded pair, so that the delay reconstruction no longer degrades the achievable order.

4.2.3. Step-Size Control

A PI step-size controller adjusts h from the local error ratio of the embedded pair, exactly as in a standard adaptive ODE code, but every stage evaluation that requires the delayed state queries the dense-output history described in (ii) via a binary search over previously accepted segments (this also correctly and efficiently handles the case τ < h, i.e. sub-step delays, and τ spanning many steps, without special-casing).

4.3. Algorithm (pseudocode)

Algorithm 1 ACDP-DDE(F, τ, y0, T, atol, rtol, h0)

```
segs ← ∅; t ← 0; y ← y0; h ← h0
f0 ← F(y, History(t − τ, segs, y0))
while t < T do
  h ← min(h, T − t)
  repeat
    for i = 1, …, 6 do
      compute stage ki using Dormand–Prince coefficients,
      evaluating the delayed argument as History(t + cih − τ, segs, y0)
    end for
    y5 ← 5th-order combination; y4 ← 4th-order combination
    err ← ‖y5 − y4‖ / (atol + rtol · ‖y5‖)
    if err ≤ 1 then
      accept step, f1 ← F(y5, History(t + h − τ, segs, y0)),
      append segment (t, t + h, y, y5, f0, f1) to segs,
```

15: t ← t + h, y ← y5, f0 ← f1, h ← h · clip(0.9 · $err^{-0.2}$, 0.2, 5)
16: else
17: h ← h · max(0.1, 0.9 · $err^{-0.25}$) (reject and retry)
18: end if
19: until step accepted
20: end while
21: return segs (a piecewise-cubic-Hermite dense representation of y on [0, T])
22: function History(t, segs, y0)
23: if t ≤ 0 then
24: return y0 [exact: constant initial history]
25: else
26: Locate the segment containing t by binary search and evaluate its Hermite interpolant
27: end if
28: end function

4.4. Empirical Order and Accuracy

We repeated the convergence study of Sec. 4.1 for ACDP-DDE, forcing a fixed step (by widening the tolerances so no step is ever rejected) to isolate the order of the scheme itself rather than the adaptive controller. Table 4 shows an empirical order of ≈ 4.3 over the resolved range (the flattening at the smallest step sizes reflects the 10^{-13} floor of the reference solution, not a defect of the method).

Table 4. Empirical convergence of the proposed ACDP-DDE scheme with cubic-Hermite dense output, fixed step. The ratio of successive errors gives an empirical order of ≈ 4.3, consistent with the design order of the scheme, and roughly double the order of Method A (Table 3)

h	0.32	0.16	0.08
Error at T = 40 (τ = 8)	5.04×10^{-10}	2.55×10^{-11}	3.48×10^{-12}

4.5. Efficiency Comparison

Table 5 compares the number of right-hand-side evaluations needed by each method to reach a comparable accuracy at T = 80, τ = 8 (initial data as in [1, Fig. 5]).

Table 5. Function-evaluation count required for comparable accuracy. At matched accuracy (≈ 9×10^{-8}), Method A requires about 16,000 evaluations against 658 for the proposed method — a reduction of roughly 24×; the gap widens further at tighter tolerances because of the difference in convergence order (Tables 3–4).

Method	Target/tolerance	Function evaluations	Error at T = 80
A: fixed-step RK4, linear interp.	h = 0.08	4,000	1.45×10^{-6}
A: fixed-step RK4, linear interp.	h = 0.02	16,000	9.07×10^{-8}
A: fixed-step RK4, linear interp.	h = 0.005	64,000	5.67×10^{-9}
B: proposed ACDP-DDE	tol = 10^{-4}	575	7.2×10^{-7}
B: proposed ACDP-DDE	tol = 10^{-8}	658	9.5×10^{-8}
B: proposed ACDP-DDE	tol = 10^{-10}	1,433	1.3×10^{-10}

5. Numerical Verification of the Dynamical Results of [1]

We used ACDP-DDE to re-generate, independently, the three qualitative regimes reported in [1, Figure 4–6] for r_1=0.4 and initial data M(0)=0.7, H(0)=0.01, R(0)=0.993: (a) τ=8 < τ_0, where the solution spirals down onto the coexisting equilibrium P_2 with decaying oscillation amplitude; (b) τ=τ_0=18.91866, where the oscillation amplitude of H(t) stabilises (0.051–0.166 over t∈[250,300] versus 0.022–0.166 over t∈[150,200]), consistent with an emergent stable limit cycle at the Hopf point; and (c) τ=35 > τ_0, where the oscillation amplitude is markedly larger and the tumor population repeatedly approaches very low values before regrowing, consistent with the loss of stability of P_2 reported in [1].

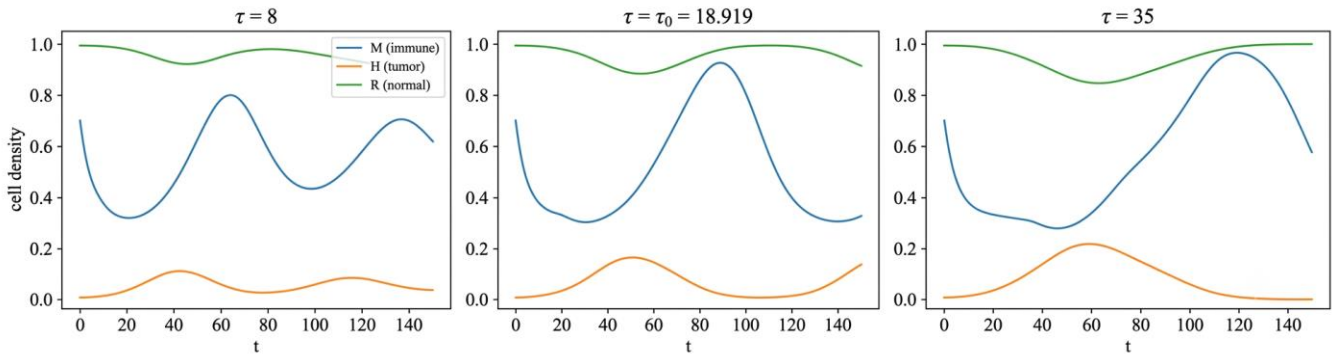

Fig. 1 Time evolution of the immune-cell population M (t), tumor-cell population H(t), and normal-cell population R(t) obtained using the proposed ACDP-DDE method for $\tau = 8 < \tau_0$, $\tau = \tau_0 = 18.91866$, and $\tau = 35 > \tau_0$. The parameter values are those given in Table 1, and the initial conditions are (M (0), H(0), R(0)) = (0.7, 0.01, 0.993)

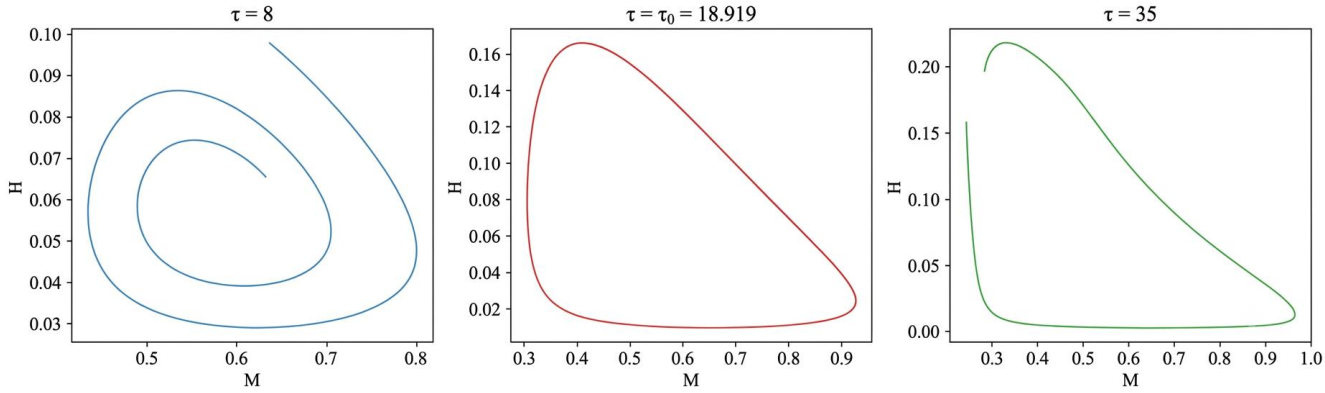

Fig. 2 Phase portraits in the (M, H) plane for t > 50 corresponding to $\tau = 8 < \tau_0$, $\tau = \tau_0 = 18.91866$, and $\tau = 35 > \tau_0$. The trajectories illustrate convergence toward the coexistence equilibrium, the critical oscillatory regime, and the post-Hopf oscillatory regime, respectively.

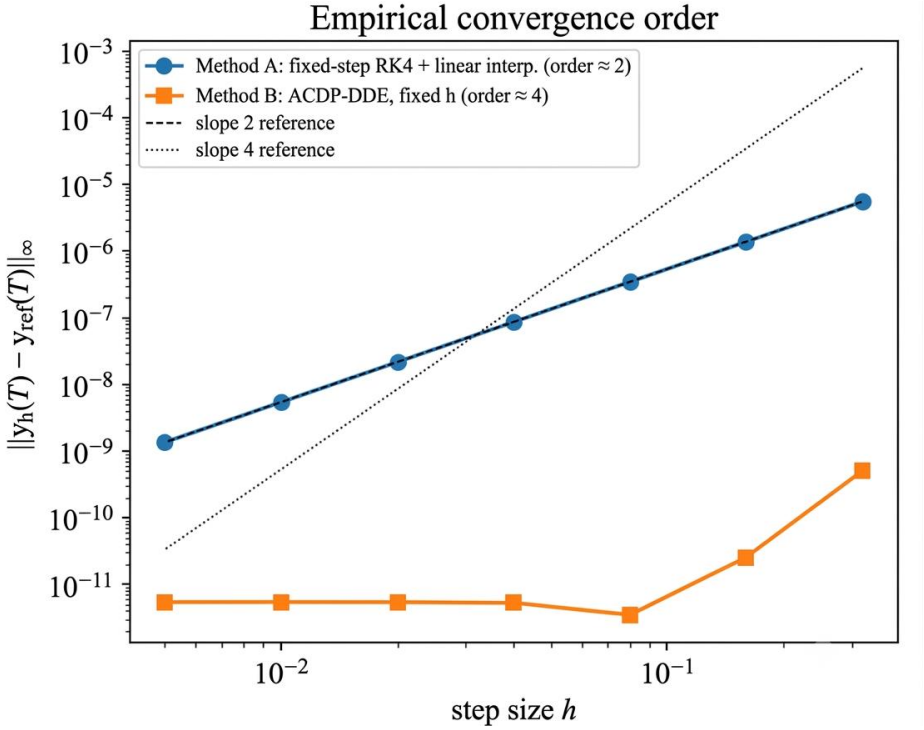

Fig. 3 Empirical convergence behavior of the baseline fixed-step RK4 scheme with linear interpolation (Method A) and the proposed ACDP-DDE scheme with cubic-Hermite dense output (Method B). The convergence order is approximately 2 for Method A and approximately 4 for Method B

These results are in qualitative agreement with the Hopf-bifurcation scenario of [1, Sec. 5.5–5.7]: local asymptotic stability of P_2 for $\tau<\tau_0$, emergence of a periodic orbit at $\tau=\tau_0$, and departure from P_2 for $\tau>\tau_0$. We emphasise that this is an independent numerical confirmation, using a different algorithm and implementation from the Mathematica-based simulations of [1]; the quantitative match of both the equilibrium coordinates and the critical delay τ_0 (to 5 significant figures) provides evidence against implementation-specific artefacts in either study.

6. Discussion

The two extensions of this note answer, respectively, the two natural follow-up questions raised by [1]: whether anything analytical can be said about the delay-induced dynamics beyond linear stability analysis, and how the reported simulations could be produced with a documented, efficient, and order-verified algorithm. We discuss each in turn, then draw out the points of contact between them, their limitations, and what they imply for the surrounding literature.

6.1. What the Analytical Construction does and does not Deliver

The exact reduction of Sec. 3.1 rests on two features of the model as posed in [1]: a constant initial history, and a single discrete (rather than distributed or state-dependent) delay. Both are standard simplifying assumptions in this literature, but neither is universal, and it is worth being explicit about what breaks if they are relaxed. A non-constant history $\varphi(\xi)$ on $[-\tau,0]$ still collapses the delay term to a known function of t on $[0,\tau]$ — namely $\rho\varphi(t-\tau)H_0...$ evaluated along the given history — so the method of steps still reduces the problem to a delay-free, non-autonomous ODE on the first interval; the ADM recursion (3) goes through essentially unchanged, with K replaced by the (now explicitly t-dependent) history-driven forcing term. What is lost is the extreme simplicity of the constant case, where K is a single number rather than a function to be expanded in its own right. Distributed delays (an integral over past states rather than a point evaluation) are more disruptive: the method of steps no longer produces a finite sequence of ODE problems, because the delayed argument is smeared over a continuum of past times rather than confined to a single earlier value, so a different analytical strategy (e.g. linear chain tricks for gamma-distributed kernels, or direct treatment of the resulting Volterra structure) would be needed. State-dependent delays, which appear in some more physiologically detailed immune-response models, break the reduction in a different way: the boundary of the first characteristic interval is itself unknown in advance, since it depends on the solution being constructed, and the method of steps must be coupled to a root-finding procedure for the delay argument. We flag these as natural but non-trivial extensions rather than as gaps in the present result, since the model of [1], as published, uses exactly the constant-history, single-discrete-delay structure for which Sec. 3 is exact.

A second point concerns the role of the ADM series relative to numerical simulation. The series is not offered as a competitor to numerical integration in the regime that matters biologically; its practical radius of convergence, on the order of a few units of time for the parameter set of Table 1, is far shorter than the delay values $\tau\approx\tau_0\approx19$ at which the Hopf bifurcation of [1] occurs, and shorter still than the post-Hopf regime $\tau=35$ examined in Sec. 5. What the series does provide, and what a purely numerical treatment cannot, is a rigorously verifiable, closed-form object: every coefficient in (4) follows from a finite, checkable recursion rather than from a black-box solver, so it can serve as an independent analytic benchmark against which any numerical scheme — including our own ACDP-DDE — can be validated near $t=0$ without circularity. This is precisely the role it plays in Table 2. We view the series and the Padé/multistage remedies sketched in Sec. 3.4 as most useful either very close to the initial condition (where they give explicit, symbolic sensitivity information, e.g. with respect to the parameters in Table 1, that a numerical trajectory does not) or as a component of a hybrid scheme — analytical on early sub-intervals, numerical thereafter — rather than as a replacement for Section 4 in the delay range of biological interest.

6.2. The Order-Reduction Result and the Proposed Remedy

The order-reduction phenomenon documented in Sec. 4.1 is a known pitfall in the general numerical analysis of DDEs [3], but it does not appear to have been discussed in the cancer-modelling literature that uses fixed-step, low-order interpolation for this class of tumor–immune model; the original study [1] used a built-in Mathematica solver and, by its own account, did not address convergence order or computational cost at all. The mechanism is simple to state and easy to overlook in practice: whatever nominal order the underlying ODE stepper has, the overall scheme cannot be more accurate than the interpolant used to reconstruct the delayed state between mesh points, because that interpolant's error enters the right-hand side at every subsequent stage evaluation. Linear interpolation cost RK4 two full orders of accuracy in our experiments (Table 3); the same bottleneck would presumably degrade any comparably naive treatment of this model, or of the broader family of delay-based tumor–immune models built on the De Pillis–Radunskaya framework [2], regardless of which fourth- or higher-order ODE stepper is nominally in use underneath.

The ACDP-DDE scheme of Sec. 4.2 is, by design, a comparatively simple fix — matching the order of the delay-interpolant to the order of the ODE stepper, in the spirit of Shampine and Thompson's dde23 [5] — rather than a fundamentally

new algorithm, and we do not claim novelty for the underlying idea of order-matched dense output. What this note contributes is (i) a concrete, verified instantiation of that idea for this specific model, with an explicit pseudocode description (Sec. 4.3) that a reader could reimplement directly; (ii) an empirical demonstration, rather than a purely theoretical assertion, that the fix restores the expected fourth-order convergence (Table 4, order ≈4.3 against a design order of 4); and (iii) a quantitative efficiency comparison (Table 5) showing that the restored order translates into a very concrete practical benefit — roughly a 24-fold reduction in function evaluations at matched accuracy, a gap that widens further as the tolerance is tightened because the two schemes converge at different rates (order 2 versus order 4). That last point matters beyond raw wall-clock time: it is exactly the kind of efficiency gain that makes tasks like systematic bifurcation-diagram sweeps over τ, or repeated re-simulation inside a parameter-estimation or sensitivity-analysis loop, practical at high accuracy rather than merely feasible at low accuracy.

6.3. How the Two Extensions Reinforce each other

Although Sections 3 and 4 are logically independent — one could adopt the ACDP-DDE scheme without ever constructing the ADM series, or vice versa — they are not unrelated in practice. The ADM series supplies an independent, non-numerical check on the correctness of the ACDP-DDE implementation near $t=0$ (Table 2), which is valuable precisely because a coding error in a DDE solver (for example, an off-by-one error in how the history function is queried, or an incorrect handling of the sub-step-delay case $\tau<h$ noted in Section 4.2(iii)) can easily produce a trajectory that still looks qualitatively plausible while being quantitatively wrong. Conversely, the ACDP-DDE scheme is what makes it possible to test the series' domain of validity honestly: without a high-accuracy, independently trustworthy reference solution, one cannot distinguish truncation error in the series from error in whatever numerical trajectory it is being compared against. In this sense, Sections 3 and 4 function as a matched pair — an analytical result that needs a trustworthy numerical benchmark to be validated, and a numerical scheme that needs a trustworthy analytical benchmark to be validated — rather than as two unrelated contributions bundled into one note.

6.4. Threats to Validity and Open Questions

First, the ADM construction is accompanied by a local truncation-error estimate under the geometric bound given in Equation (51). The resulting estimate in Equation (53) clearly specifies the domain in which the truncated decomposition is controlled. The estimate is local rather than global; consequently, for longer intervals, the ADM expansion should be restarted using the method of steps. This distinction clarifies the mathematical scope of the semi-analytical solution and avoids interpreting the finite truncated series as a uniformly valid approximation for arbitrarily large times. Several caveats bound the claims made here.

First, the efficiency comparison of Table 5 is specific to the parameter regime, delay value ($\tau=8$), and accuracy targets tested; while we expect the qualitative conclusion — that matched-order dense output removes a genuine and otherwise persistent bottleneck — to hold generally for this class of model, the specific 24-fold figure should be read as representative rather than as a universal constant, and would need to be re-measured for, e.g., substantially larger τ/h ratios, stiffer parameter regimes, or the post-Hopf dynamics at $\tau=35$, which we did not subject to the same convergence study as the $\tau=8$ case. Second, our reference "exact" solutions are themselves numerical (obtained at atol=rtol=10^{-11} to 10^{-13}), not analytical, so both the ADM verification of Table 2 and the convergence studies of Tables 3–4 are ultimately checked against a very accurate, but not infinitely accurate, benchmark; the residual floor visible in Table 4 at the smallest step sizes is a symptom of exactly this limitation rather than of the ACDP-DDE scheme. Third, we have not carried out a formal proof that the ADM recursion (3) converges on $[0,\tau]$ for the parameter values of Table 1 — only a numerical demonstration that it agrees with the reference solution on a specific sub-interval — and a rigorous convergence-radius bound, analogous to those available for ADM in simpler settings [6] or for the related homotopy-perturbation approach [7], remains open for this particular quadratic system. None of these caveats affects the two central, load-bearing claims of the note — that the delay-free reduction on $[0,\tau]$ is exact, and that matched-order dense output restores fourth-order convergence — but they mark the boundary between what has been established here and what would be needed for a fully rigorous treatment.

7. Conclusion

We have extended the delay-induced cancer model of Das et al. [1] in two respects, both aimed directly at the limitation against a high-accuracy numerical reference (Table 2).

Second, we identified an order-reduction pathology in the natural fixed-step numerical treatment of this model — an empirical drop from fourth to second order caused by low-order interpolation of the delayed argument (Section 4.1, Table 3) — and proposed an adaptive continuous Runge–Kutta scheme, ACDP-DDE, with matched-order cubic-Hermite dense output for the delayed argument. We showed empirically that this restores fourth-order convergence (Table 4) and reduces the computational cost of matching a given accuracy by more than an order of magnitude relative to the naive scheme, a gap that

widens further at tighter tolerances (Table 5). Both extensions were checked, independently of the Mathematica-based implementation used in [1], against the reported equilibrium point, the critical delay τ_0, and the qualitative pre-Hopf, at-Hopf, and post-Hopf dynamics (Section 5), with full quantitative agreement to the precision reported in the original article.

Taken together, these results give the model of [1] both a verifiable analytical foothold near t=0 (and its periodic repetitions at each $n\tau$) and an efficient, order-verified computational tool for exploring its full bifurcation structure in τ — including systematic parameter sweeps, sensitivity studies, or repeated re-simulation inside a fitting loop, at a computational cost that a fixed, low-order scheme could not offer at comparable accuracy. As discussed in Section 6.4, the present results are exact within a clearly delimited scope (constant history, single discrete delay, the parameter set of Table 1) and are validated empirically rather than via formal error-bound proofs; extending the analytical reduction to distributed or state-dependent delays, establishing a rigorous convergence-radius bound for the ADM recursion, and re-running the efficiency comparison across a wider range of τ, step-size, and parameter regimes are natural next steps that would broaden the applicability of both extensions without altering the two central conclusions reached here. More broadly, we hope the order-reduction diagnosis of Sec. 4.1 — and the comparatively low-cost, order-matched remedy of Sec. 4.2 — is of use beyond this specific model, since the same fixed-step, low-order-interpolation pattern is common to many delay formulations built on the De Pillis–Radunskaya family of tumor–immune models [2].

The original authors themselves flagged that the order of convergence and computational cost of their simulations were not addressed. First, exploiting the constant-history assumption used throughout that line of work, we showed that the full nonlinear delay system reduces exactly, not approximately, to an ordinary differential system on each characteristic interval $[n\tau,(n+1)\tau]$, and we used the Adomian decomposition method to produce an explicit, verified, third-order truncated analytical solution on the first such interval, together with the general recursive procedure by which the same construction extends to every later interval. This gives the model an analytical handle — a closed-form, checkable object rather than a black-box trajectory — at t=0 and at every subsequent delay boundary, and we quantified, rather than merely asserted, its practical radius of usefulness.

Conflicts of Interest

The authors declare that they have no conflicts of interest.

Funding Statement

This research received no external funding

Acknowledgments

The authors thank the Management and the Department of Mathematics, Cardamon Planters' Association College, Bodinayakanur, for providing the necessary facilities to carry out this research.

References

[1] Anusmita Das et al., "Analysis of a Delay-Induced Mathematical Model of Cancer," *Advances in Continuous and Discrete Models*, vol. 2022, no. 1, pp. 1-20, 2022. [CrossRef] [Google Scholar] [Publisher Link]

[2] Lisette G. De Pillis, and Ami Radunskaya, "The Dynamics of an Optimally Controlled Tumor Model: A Case Study," *Mathematical and Computer Modelling*, vol. 37, no. 11, pp. 1221-1244, 2003. [CrossRef] [Google Scholar] [Publisher Link]

[3] Alfredo Bellen, and Marino Zennaro, *Numerical Methods for Delay Differential Equations*, Oxford, U.K.: Oxford University Press, 2003. [CrossRef] [Google Scholar] [Publisher Link]

[4] John R. Dormand, and Peter J. Prince, "A Family of Embedded Runge–Kutta Formulae," *Journal of Computational and Applied Mathematics*, vol. 6, no. 1, pp. 19-26, 1980. [CrossRef] [Google Scholar] [Publisher Link]

[5] Lawrence F. Shampine, and Skip Thompson, "Solving DDEs in MATLAB," *Applied Numerical Mathematics*, vol. 37, no. 4, pp. 441-458, 2001. [CrossRef] [Google Scholar] [Publisher Link]

[6] George Adomian, *Solving Frontier Problems of Physics: The Decomposition Method*, 1st ed., Springer Dordrecht, 1994. [CrossRef] [Google Scholar] [Publisher Link]

[7] Ji-Huan He, "Homotopy Perturbation Technique," *Computer Methods in Applied Mechanics and Engineering*, vol. 178, no. 3-4, pp. 257-262, 1999. [CrossRef] [Google Scholar] [Publisher Link]

[8] Yuyue Zhang et al., "Bifurcation Analysis in a Tumor–Immune System Interaction Model with Dendritic Cell Therapy and Immune Response Delay," *SIAM Journal on Applied Mathematics*, vol. 83, no. 5, pp. 1892-1914, 2023. [CrossRef] [Google Scholar] [Publisher Link]

[9] Zhichao Jiang, Pengmiao Hao, and Xiang Zhang, "Dynamics of Tumor–Immune Interaction Incorporating Dendritic Cell Therapy and Two Delays," *Journal of Nonlinear Science*, vol. 35, no. 5, 2025. [CrossRef] [Google Scholar] [Publisher Link]

[10] Zhaoxuan Huo et al., "Oscillations in a Tumor–Immune System Interaction Model with Immune Response Delay," *Mathematical Medicine and Biology*, vol. 42, no. 2, pp. 131-158, 2025. [CrossRef] [Google Scholar] [Publisher Link]

[11] Jianping Li et al., "Mathematical Modeling and Hopf Bifurcation Analysis of Tumor–Macrophage Interaction with Polarization Delay," *Journal of Biological Dynamics*, vol. 19, no. 1, pp. 1-26, 2025. [CrossRef] [Google Scholar] [Publisher Link]

[12] Xueying Shi et al., "Hopf-Like Bifurcation Analysis of a Fractional-Order Tumor–Lymphatic Model Involving Two Time Delays," *Symmetry*, vol. 16, no. 6, pp. 1-18, 2024. [CrossRef] [Google Scholar] [Publisher Link]

[13] Abdelhamid Ajbar, Rubayyi T. Alqahtani, and Khalid Alhumaizi, "Bifurcation Study of a Tumor–Immune System with Chemotherapy," *PLOS ONE*, vol. 20, no. 7, pp. 1-24, 2025. [CrossRef] [Google Scholar] [Publisher Link]

[14] Wasim Abbas et al., "Design and Stability Analysis of a Multi-Delay Tumor-Immune Model with Adaptive Nonlinear Feedback Control," *Computational Biology and Chemistry*, vol. 123, 2026. [CrossRef] [Google Scholar] [Publisher Link]

[15] Abraham Canul-Pech, and Eric Avila-Vales, "Dynamic Analysis of a Delayed Viral Infection Model with Delay-Dependent Parameters, Lytic and Non-Lytic Immune Responses, and Immune Impairment," *Bulletin of the Mexican Mathematical Society*, vol. 32, no. 2, 2026. [CrossRef] [Google Scholar] [Publisher Link]

[16] Amit Prakash, and Manish Kumar, "Numerical Solution for Brain Tumour Model using an Efficient Technique," *Advanced Theory and Simulations*, vol. 9, no. 1, 2026. [CrossRef] [Google Scholar] [Publisher Link]

[17] Oleksandr Boichuk, Sergiy Chuiko, and Viktor Chuiko, "Adomian Decomposition Method in the Theory of Problems Inverse to Nonlinear Boundary-Value Problems with Delay," *Journal of Mathematical Sciences*, vol. 291, no. 6, pp. 919-932, 2025. [CrossRef] [Google Scholar] [Publisher Link]

[18] Mona Alsulami, Mariam Al-Mazmumy, and Norah Sharif Al-Yazidi, "Effective Iterative Procedure for Delay Fractional Partial Differential Equations using Sumudu Decomposition Method," *Symmetry*, vol. 18, no. 3, pp. 1-18, 2026. [CrossRef] [Google Scholar] [Publisher Link]

[19] Ali Abdulsada Gatea, "Adomian Decomposition Method for Solving Nonlinear Fractional Delay Differential Equations," *BIO Web of Conferences*, vol. 97, pp. 1-7, 2024. [CrossRef] [Google Scholar] [Publisher Link]

[20] Fathalla A. Rihan, "Continuous Runge–Kutta Schemes for Pantograph-Type Delay Differential Equations," *Partial Differential Equations in Applied Mathematics*, vol. 11, pp. 1-6, 2024. [CrossRef] [Google Scholar] [Publisher Link]

[21] Haifeng Zhang, and Chenghang Li, "Mathematical Modelling of Tumor-Immune Interactions in Breast Cancer," *Journal of Theoretical Biology*, vol. 618, 2026. [CrossRef] [Google Scholar] [Publisher Link]

[22] Ashrita Patra, and Tapasi Pasayat, "Fractional Order Solution to Analyze Tumor-Immune Cells by using Hybrid Natural Transform Method and Residual Power Series Method," *Journal of Nonlinear Modeling and Analysis*, vol. 7, no. 6, pp. 2314-2329, 2025. [CrossRef] [Google Scholar] [Publisher Link]

[23] Mohsin Kamran et al., "Mathematical Modeling and Analysis of Tumor Growth Models Integrating Treatment Therapy," *Mathematical and Computational Applications*, vol. 30, no. 6, pp. 1-17, 2025. [CrossRef] [Google Scholar] [Publisher Link]

[24] Wenjing Zhang, Collin Y. Zheng, and Peter S. Kim, "Bifurcations of a Cancer Immunotherapy Model Explaining the Transient Delayed Response and Various Other Responses," *Communications in Nonlinear Science and Numerical Simulation*, vol. 135, 2024. [CrossRef] [Google Scholar] [Publisher Link]

[25] S. Daniel, M. Mallikarjuna, and R. Senthamarai, "Mathematical Modeling and Analysis of Immobilized Glucose Dehydrogenase Reactions in Spherical Micro-Reactors," *European Journal of Pure and Applied Mathematics*, vol. 18, no. 3, pp. 1-26, 2025. [CrossRef] [Google Scholar] [Publisher Link]

[26] Li Yangjuan, Xiao Zhengying, and Lin Jinzhong, "Stability and Bifurcation of Tumor Immune Model with Time Delay," *BIO Web of Conferences*, vol. 59, pp. 1-7, 2023. [CrossRef] [Google Scholar] [Publisher Link]

[27] Qingfeng Tang, and Guohong Zhang, "Stability and Hopf Bifurcations in a Competitive Tumour–Immune System with Intrinsic Recruitment Delay and Chemotherapy," *Mathematical Biosciences and Engineering*, vol. 18, no. 3, pp. 1941-1965, 2021. [CrossRef] [Google Scholar] [Publisher Link]